SEMARAK ILMU PUBLISHING

CFD Letters

Journal homepage:
https://semarakilmu.com.my/journals/index.php/CFD_Letters/index
ISSN: 2180-1363

# Numerical Simulation of Droplet Coalescence using Meshless Radial Basis Function and Domain Decomposition Method

Eko Prasetya Budiana[1,*], Pranowo[2], Catur Harsito[3], Dominicus Danardono Dwi Prija Tjahjana[1], Syamsul Hadi[1]

[1] Department of Mechanical Engineering, Faculty of Engineering, Universitas Sebelas Maret, Surakarta, Indonesia
[2] Department of Informatics, Faculty of Engineering, Universitas Atma Jaya Yogyakarta, Indonesia
[3] Mechanical Engineering of Vocational School, Universitas Sebelas Maret, Surakarta, Indonesia

**ARTICLE INFO**

***Article history:***
Received 12 February 2024
Received in revised form 23 May 2024
Accepted 14 June 2024
Available online 31 October 2024

***Keywords:***
Droplet Coalescence; Fractional Step; Radial Basis Function; Cahn-Hilliard Equations

**ABSTRACT**

The present investigation of the dynamic two-binary droplet interactions has gained attention since its use to expand and improve several numerical methods. Generally, its interactions are classified into coalescence, bouncing, reflective, and stretching separation. This study simulated droplet coalescence using the meshless radial basis function (RBF) method. These methods are used to solve the Navier-Stokes equations combined with the Cahn-Hilliard equations to track the interface between two fluids. This work uses the fractional step method to calculate the pressure-velocity coupling in the Navier-Stokes equations. The numerical results were compared with the available data in the literature to validate the proposed method. Based on the validation, the proposed method conforms well with the literature. To identify further coalescence characteristics, the model considered different values in viscosity (2, 4, and 8 cP), collision velocity (1.5 m/s and 3 m/s), and surface tension (0.014, 0.028, and 0.056 N/m) parameters. The increasing viscosity was linearly proportional to the collision time, whereas increased surface tension and collision velocity shortened the collision time.

## 1. Introduction

Droplet coalescence plays an essential role in many engineering applications, such as spray cooling [1], desalination [2], fuel combustion [3], petroleum transporting pipelines [4], and coating [5]. Therefore, many researchers have studied those phenomena experimentally and numerically. In the oil industry, the merging of dispersed water droplets in crude oil is described as water coalescence [6]. In the formation of the raindrop, droplet collision takes place naturally [7].

Several numerical experiments were used to simulate two-phase flow problems. Gomes *et al.,* [8] applied FLUENT software, a CFD package based on the finite volume method, to calculate pressure drop in the oscillating water column device. Their study defined the interface of two fluids using the Volume of Fluid (VOF) method. Mason *et al.,* [9] numerically studied the collisions of two droplets

* *Corresponding author.*
*E-mail address: ekoprasetya@staff.uns.ac.id (Eko Prasetya Budiana)*

https://doi.org/10.37934/cfdl.17.4.117

using a multi-scale simulation method. They proposed the Volume of Fluid (VOF) method to capture the interface of two fluids, resulting in the droplet evolution matching the experimental result of Pan *et al.,* [10]. Mohammadi *et al.,* [11] investigated the collision of water droplets in oil using the finite volume method and the Volume of Fluid (VOF) method to track the interface of two fluids. The effects of collision velocity, off-center collision parameter, viscosity, and surface tension were considered. Mansouri *et al.,* [12] proposed a numerical simulation of water droplet collisions in oil. The collisional behavior of the droplet was investigated numerically using a commercial CFD code Fluent 14, and the interface of two fluids was approached using the Volume of Fluid (VOF) method.

Fluid flow problems have usually been simulated using conventional numerical methods based on finite difference [13], finite volume [14], and finite element [15] methods. The natural convection of viscous incompressible fluid in a finite domain has been investigated using the control volume method proposed by Perepechko *et al.,* [16]. Their study has applied the technique to simulate heat-mass transfer processes in incompressible media with variable viscosity and thermal conduction. The difficulty in the mesh-based method was the high mesh quality requirement in the computational domain and boundary. To handle the difficulty, various meshless methods such as meshless local Petrov-Galerkin (MLPG) [17], meshless backward subtititution method, and radial basis function (RBF) [18], have been developed in the last decade. Najafi *et al.,* [19] applied meshless local Petrov-Galerkin (MLPG) to handle the heat transfer problem of natural convection at high Rayleigh numbers. Using their method, they could simulate the natural convection in a square cavity for Ra =$10^8$, in a concentric square outer cylinder and circular inner cylinder annulus for Ra = $10^7$, and in a two concentric circular cylinder annulus for Ra = $10^5$. Their works used the fractional step method to discretize the momentum equations to obtain the pressure and velocity terms. The RBF method has been developed to solve the partial differential equations [20] and Navier-Stokes equations [21]. Ma *et al.,* [22] introduced the meshless backward substitution method (BSM) to solve the time-harmonic elastic wave problems. They concluded that the BSM can provide more precise solutions for problems involving regular and irregular domains at various frequencies. Zang *et al.,* [23] also used the meshless backward substitution method (BSM) to simulate two-dimensional incompressible flows. Their investigations show that this method has high computational efficiency and better accuracy than other RBF-based methods. Zheng *et al.,* [24] introduced the local radial basis function-parameterized level set method (RBF-PLSM) to solve various partial differential equations. Their numerical results show that the method is more efficient than the standard RBF method. Soleymani *et al.,* [25] used the radial basis function-generated finite difference (RBF-FD) scheme in the presence of the generalized multiquadric function (GMQ) to solve the partial integro-differential equation (PIDE) and partial differential equation (PDE) models. In 2023, Soleymani *et al.,* [26] also used meshless radial basis function-generated finite difference (RBF-FD) based on the inverse quadratic IQ function to solve the partial differential equation (PDE) model. The numerical results show the effectiveness and accuracy of the numerical scheme.

Table 1 provides information on the available literature on the numerical simulation of fluid flow problems. In that table, the summary includes the simulation of single-phase and two-phase flow problems, such as natural convection and droplet coalescence. There are also several numerical studies on droplet coalescence using different numerical methods.

Combining the RBF with the DDM was a reasonable approach, particularly in narrowing the gap in implementing and developing numerical method types, which leads to accommodating high-precision outcomes. Darell *et al.,*'s [27] study proved the high precision of this meshless RBF by comparing it to traditional mesh-based methods used in Comsol and Fluent. Past studies have successfully conducted a coalescence droplet model using various numerical approaches. For instance, Barosan *et al.,*'s [28] research successfully solves the droplet coalescence model using the

diffuse interface spectral element method. That study's approach, which uses grid refinement and has a complex domain structure, makes the model challenging to understand. Therefore, presenting a radial basis function with the most straightforward uniformly structured grid and computational efficiency proved challenging. In this study, the combination of meshless RBF and DDM is proposed to solve droplet coalescence phenomena. The Navier-Stokes equation governs this related phenomenon in terms of primitive variables and the Cahn-Hilliard equation. The Cahn-Hilliard equation is considered to capture the evolution of the interface of the droplets. The factional step numerical procedure solves pressure-velocity coupling in the Navier-Stokes equation. The main contribution of the present numerical RBF-DDM method consists of three advantages. Firstly, the implication of meshless RBF offers an advantage in accommodating the mesh generation difficulty. Secondly, to solve the problem efficiently, the DDM divides the large-scale computational domain into many small subdomains. Lastly, in the Cahn-Hilliard equations, the interface changes are defined automatically, making it unnecessary to track the interface explicitly [29]. Bates *et al.,* [30] and Anderson *et al.,* [31] proposed that the Cahn-Hilliard equations are thermodynamically consistent and capture the interface between two fluids.

**Table 1**
Summary of investigation on the numerical solution of fluid flow problems

| Ref. | Method | Remarks |
|---|---|---|
| [8] | FLUENT software, and Volume of Fluid (VOF) method | The software solves the pressure drop in an oscillating water column device. The interface of two fluids was defined using the Volume of Fluid (VOF) method. |
| [16] | control volume method | The natural convection of viscous compressible fluid in a finite domain has been investigated using the control volume method. |
| [19] | meshless local Petrov–Galerkin method | The method was used to solve natural convection heat transfer at high Rayleigh numbers in a square cavity and circular annulus. The fractional step method was applied to discretize the momentum equations to obtain the pressure and velocity variables. |
| [9] | multi-scale simulation method and volume of fluid (VOF | The evolution of the droplet interface in their work is in good accordance with the experimental results of Pan *et al.,* [9]. |
| [11] | finite volume method, and Volume of Fluid (VOF) method | The study is based on the finite volume method and the Volume of Fluid (VOF) method to track the interface of two fluids. The effects of collision velocity, off-center collision parameter, viscosity, and surface tension were considered |
| [12] | Fluent 14, and Volume of Fluid (VOF) method | The water droplet collisions in oil were investigated using commercial CFD code Fluent 14. The interface of two fluids was approached using the Volume of Fluid (VOF) method. |

## 2. Methodology

### *2.1 Governing Equations and Problem Definition*

The governing equations for the coalescence of the droplets are determined by the Navier-Stokes and Cahn–Hilliard equations, which are given as:

$$\frac{\partial \mathbf{u}}{\partial t} + (\mathbf{u}.\nabla)\mathbf{u} = -\frac{1}{\rho(c)}\nabla p + \frac{\eta(c)}{Re.\rho(c)}\nabla^2 u + SF(c) \quad (1)$$

$$\nabla.\mathrm{u} = 0 \quad (2)$$

Where x and y are spatial coordinates in horizontal and vertical directions, corresponding to velocities u and v with pressure (P). This momentum equation incorporates the external surface force (SF) acting on the droplet contact.

$$\frac{\partial c}{\partial t} + \mathbf{u}\nabla c = \frac{1}{Pe}\nabla^2 \mu \tag{3}$$

$$\mu = c^3 - c - Ch^2\nabla^2 c \tag{4}$$

$$\rho(c) = \left(\frac{c+1}{2}\right) + \frac{\rho_o}{\rho_w}\left(\frac{1-c}{2}\right) \tag{5}$$

$$\eta(c) = \left(\frac{c+1}{2}\right) + \frac{\eta_o}{\eta_w}\left(\frac{1-c}{2}\right) \tag{6}$$

The Cahn-Hilliard equations Eq. (3) and Eq. (4) accommodate the droplet phases interact. Where c is the concentration, $\rho$ is the density, o, and w are the indices for oil and water, and $\eta$ is the kinematic viscosity. The above equations are obtained using the following dimensionless Eq. (7). Which represents the dimensionless values. The variables t, Do, and $V_o$ are time, initial droplet size, and initial droplet velocity, respectively.

$$\begin{aligned} &x' = \frac{x}{D_o} \quad u' = \frac{u}{V_o} \quad t' = \frac{tVo}{Do}, \quad \rho' = \frac{\rho}{\rho_o}, \\ &p' = \frac{p}{\rho_o Vo^2} \quad \eta' = \frac{\eta}{\eta_o} \quad SF(c) = \frac{\rho\mu}{WeCh}\nabla c \quad \mu' = \frac{\mu}{\mu_o} \end{aligned} \tag{7}$$

The Reynolds number (Re), Weber number (We), Cahn number (Ch), and Peclet number (Pe) are defined using the equation below. In this equation, $\xi$ represents the interface thickness, and $\sigma$ represents the surface tension.

$$Re = \frac{\rho_o VoDo}{\eta_o} \tag{8}$$

$$We = \frac{\rho_w Vo^2 Do}{\sigma} \tag{9}$$

$$Ch = \frac{\xi}{Do} \tag{10}$$

$$Pe = \frac{VoDo}{M\mu_o} \tag{11}$$

The present study defines the initial concentration conditions by the hyperbolic tangent function (Eq. (12)), with H and L representing the length and height domain.

$$c = tanh\left(\frac{D_o}{2} - \frac{\sqrt{\left(x-\left(\frac{L}{2}-D_o\right)\right)^2+\left(y-\frac{H}{2}\right)^2}}{2\sqrt{2}Ch}\right) + tanh\left(\frac{D_o}{2} - \frac{\sqrt{\left(x+\left(\frac{L}{2}-D_o\right)\right)^2+\left(y-\frac{H}{2}\right)^2}}{2\sqrt{2}Ch}\right) + 1 \tag{12}$$

The computational domain is described in Figure 1. The figure shows two droplets that were utilized to model the numerical cases of the binary droplet coalescence. The periodic boundary conditions are implemented on the left and right walls, and no-slip boundary conditions are applied on the top and bottom walls.

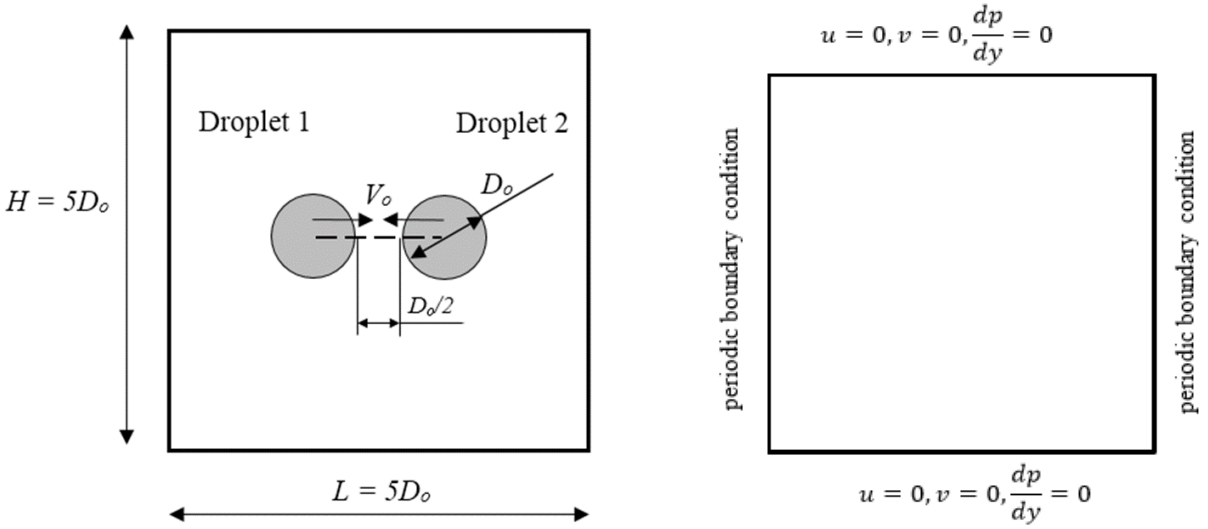


**Fig. 1.** Schematic of the (a) computational domain and (b) boundary condition

*2.2 Radial Basis Function (RBF) Method*

This section focuses on solving the governing equations of droplet coalescence using the radial basis functions (RBF) method. The advantage of the RBF method is that it does not need a mesh connection. The RBF method is a function in which the value depends only on the distance from some center point [32]. In the RBF method, a function *f* is approached as given below.

$$f = B\alpha \tag{13}$$

Where B is the interpolation matrix and $\alpha$ is the expansion coefficient, the interpolation matrix B is the N×N matrix with entries. The employed method is the multiquadric radial basis function (MQ-RBF), where the spatial derivatives' lengths between nodes are given in Eq. (14).

$$\varphi_{i,j} = \sqrt{r_{i,j}^2 + \varepsilon^2} \qquad for\ i,j = 1,2,\dots N \tag{14}$$

$$r_{i,j} = \sqrt{\left(x_i - x_j\right)^2 + \left(y_i - y_j\right)^2} \qquad for\ i,j = 1,2,\dots N \tag{15}$$

Where *r* is the distance matrix, $\varepsilon$ is the shape parameter, and $\varphi$ is the radial basis function. The first and second derivatives are expressed bellow, with x and y are the spatial vectors.

$$\left(\frac{\partial \varphi}{\partial x}\right)_{i,j} = \frac{x_i - x_j}{\sqrt{r_{i,j}^2 + \varepsilon^2}} \tag{16}$$

$$\left(\frac{\partial \varphi}{\partial y}\right)_{i,j} = \frac{y_i - y_j}{\sqrt{r_{i,j}^2 + \varepsilon^2}} \tag{17}$$

$$\left(\frac{\partial^2 \varphi}{\partial x^2}\right)_{i,j} = \frac{\left(y_i - y_j\right)^2 + \varepsilon^2}{\left(r_{i,j}^2 + \varepsilon^2\right)^{3/2}} \tag{18}$$

$$\left(\frac{\partial^2 \varphi}{\partial y^2}\right)_{i,j} = \frac{\left(x_i - x_j\right)^2 + \varepsilon^2}{\left(r_j^2 + \varepsilon^2\right)^{3/2}} \tag{19}$$

Considered with the Eq. (13), the expansion coefficient $\alpha$ is given as

$$\alpha = B^{-1} f \tag{20}$$

The RBF approximation of the first derivative $\frac{\partial f}{\partial x}$ is defined as

$$\frac{\partial f}{\partial x} = H_x \alpha \tag{21}$$

Where $H_x$ is the N×N evaluation matrix with entries $\left(\frac{\partial \varphi}{\partial x}\right)_{i,j}$, substituting Eq. (20) into Eq. (21), the equation becomes Eq. (22). Therefore, the differentiation matrix ($\mathrm{D_x} = \mathrm{H_x B^{-1}}$) governs the first derivative.

$$\frac{\partial f}{\partial x} = H_x B^{-1} f \tag{22}$$

$$\frac{\partial f}{\partial x} = D_x f \tag{23}$$

The RBF approximation of the second derivative $\frac{\partial^2 \mathrm{f}}{\partial \mathrm{x}^2}$ is expressed as

$$\frac{\partial^2 f}{\partial x^2} = H_{xx} \alpha \tag{24}$$

The $H_{xx}$ defined the N×N evaluation matrix with entries $\left(\frac{\partial^2 \varphi}{\partial x^2}\right)_{i,j}$. The Eq. (20) substituted into Eq. (24) becomes Eq. (25), where $\mathrm{D_{xx}} = \mathrm{H_{xx} B^{-1}}$ is the differentiation matrix of the second derivative. The differentiations matrix (Dy and Dyy) are calculated similarly.

$$\frac{\partial^2 f}{\partial x^2} = H_{xx} B^{-1} f \tag{25}$$

$$\frac{\partial^2 f}{\partial x^2} = D_{xx} f \tag{26}$$

### *2.3 Radial Basis Function (RBF) Method*

The domain decomposition method (DDM) is a numerical procedure that divides the large computational domain ($\Omega$) into many small subdomains ($\Omega_i$), whereas $i = 1,2, \ldots M$. M is a

number of the subdomain. Accuracy and computational efficiency for the implemented DDM were proven in the author's earlier developed model in 2023 [33]. The identical model is used to model Rayleigh Bernard convection, and then the result is compared with the previous numerical model in reference [34]. The RBF-DDM was an appropriate model with a lower node quantity than the reference, but the result had identical outcomes as long as the proposed RBF-DDM was highly efficient in solving the large dense matrix with a more efficient time in computation. Figure 2 describes the application of the domain decomposition method, in which the domain is partitioned into three subdomains. The artificial boundary $\Gamma_i$ is the boundary of $\Omega_i$ the interior of $\Omega$ and the exterior boundaries of $\Omega$ are denoted by $\partial\Omega_i \backslash \Gamma_i$. The overlapping boundaries on the subdomains are described using the multiplicative Schwarz algorithm for the elliptic PDE problem [35]. The commonly used Schwarz algorithm can be expressed as

$$\mathcal{L}U_1^n = f(x) \quad in\ \Omega_1 \tag{27}$$

$$\mathcal{B}U_1^n = g(x) \quad on\ \partial\Omega_1/\Gamma_1 \tag{28}$$

$$U_1^n = U_2^{n-1}|_{\Gamma_i} \quad on\ \Gamma_1 \tag{29}$$

and

$$\mathcal{L}U_2^n = f(x) \quad in\ \Omega_2 \tag{30}$$

$$\mathcal{B}U_2^n = g(x) \quad on\ \partial\Omega_2/\Gamma_2 \tag{31}$$

$$U_2^n = U_1^n|_{\Gamma_2} \quad on\ \Gamma_2 \tag{32}$$

where $U_i^n$ is the solution of the subdomain $\Omega_i$.

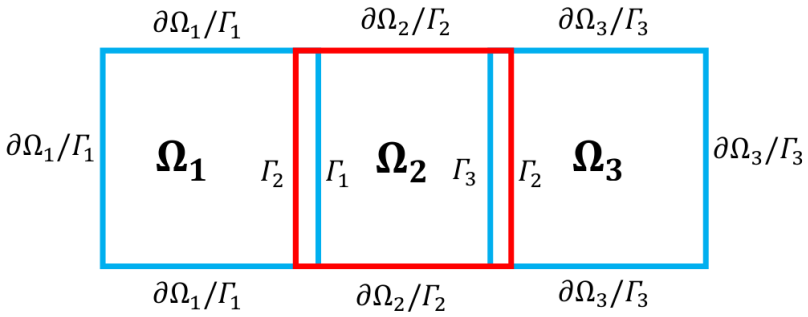


**Fig. 2.** The illustration of the domain decomposition method

### *2.4 Numerical Method*

The fractional step scheme is applied in the present study to solve the Navier-Stokes equations. The radial basis function method, which is reported in previous studies, is adopted to discretize the spatial derivatives, and the time derivative is approached using the Euler implicit scheme [36]. The application of the numerical method for the governing equation is comprehensively discussed in this section. In the first step, the pressure term is removed from the momentum equations, and the equation becomes:

$$\frac{\partial \tilde{u}}{\partial t} + u\frac{\partial \tilde{u}}{\partial x} + v\frac{\partial \tilde{u}}{\partial y} - \frac{1}{Re.\rho(c)}\left(\frac{\partial^2 \tilde{u}}{\partial x^2} + \frac{\partial^2 \tilde{u}}{\partial y^2}\right) = 0 \tag{33}$$

$$\frac{\partial \tilde{v}}{\partial t} + u\frac{\partial \tilde{v}}{\partial x} + v\frac{\partial \tilde{v}}{\partial y} - \frac{\eta(c)}{Re.\rho(c)}\left(\frac{\partial^2 \tilde{v}}{\partial x^2} + \frac{\partial^2 \tilde{v}}{\partial y^2}\right) = 0 \tag{34}$$

The Euler implicit and radial basis functions approximate the time and spatial derivatives. Therefore, the discretization form of the momentum equations is provided below.

$$\frac{\tilde{u}}{\Delta t} + u^n D_x(\tilde{u}) + v^n D_y(\tilde{u}) - \frac{1}{Re.\rho(c)}\Big(D_{xx}(\tilde{u}) + D_{yy}(\tilde{u})\Big) = \frac{u^n}{\Delta t} \tag{35}$$

$$\frac{\tilde{v}}{\Delta t} + u^n D_x(\tilde{v}) + v^n D_y(\tilde{v}) - \frac{1}{Re.\rho(c)}\Big(D_{xx}(\tilde{v}) + D_{yy}(\tilde{v})\Big) = \frac{v^n}{\Delta t} \tag{36}$$

The intermediate velocities ($\tilde{u}\ and\ \tilde{v}$) do not satisfy the continuity equation, therefore the velocities should be corrected by using the pressure term. The pressure term is calculated using Poisson equations, which are given as follow

$$\frac{\partial^2 p^{n+1}}{\partial x^2} + \frac{\partial^2 p^{n+1}}{\partial y^2} = \frac{\rho(c)}{\Delta t}\left(\frac{\partial \tilde{u}}{\partial x} + \frac{\partial \tilde{v}}{\partial y}\right) \tag{37}$$

The Poisson equation is discretized with radial basis function as given below

$$\big[D_{xx} + D_{yy}\big]\{p^{n+1}\} = \left\{\frac{\rho(c)}{\Delta t}\left(\frac{\partial \tilde{u}}{\partial x} + \frac{\partial \tilde{v}}{\partial y}\right)\right\} \tag{38}$$

The intermediate velocity defined from Eq. (36) and Eq. (37) are corrected as equations below

$$u_i^{n+1} = \tilde{u} - \frac{\Delta t}{\rho(c)} D_x(p^{n+1}) \tag{39}$$

$$v_i^{n+1} = \tilde{v} - \frac{\Delta t}{\rho(c)} D_y(p^{n+1}) \tag{40}$$

After finding the velocities (u, v) and pressure (p), the Cahn-Hilliard equations are solved to find the concentration (c) and chemical potential ($\mu$), by using the semi-implicit scheme.

$$\frac{c^{n+1} - c^n}{\Delta t} - \frac{1}{Pe}\left(\frac{\partial^2 \mu^{n+1}}{\partial x^2} + \frac{\partial^2 \mu^{n+1}}{\partial y^2}\right) = -u\frac{\partial c^n}{\partial x} - v\frac{\partial c^n}{\partial y} \tag{41}$$

$$\mu^{n+1} + C_h^2\left(\frac{\partial^2 c}{\partial x^2} + \frac{\partial^2 c}{\partial y^2}\right) = (c^n)^3 \tag{42}$$

The Picard linearization method solves the discretization in the Cahn-Hilliard equation. It's an algorithm to solve the nonlinear into linear iteration solver, as also conducted in the previous reference [28]. Therefore, both equations are solved in a coupled way.

$$\begin{bmatrix} \frac{I}{\Delta t} & -\frac{1}{Pe}\nabla^2 \\ C_h^2\nabla^2 & I \end{bmatrix}\begin{bmatrix} c^{n+1} \\ \mu^{n+1} \end{bmatrix} = \begin{bmatrix} \frac{c^n}{\Delta t} - u\frac{\partial c^n}{\partial x} - v\frac{\partial c^n}{\partial y} \\ (c^n)^3 \end{bmatrix} \tag{43}$$

The discretization forms for the Cahn-Hilliard equations are expressed as Eq. (44) where *I* is an identity matrix.

$$\begin{bmatrix} \frac{I}{\Delta t} & -\frac{DD}{Pe} \\ C_h^2 DD & I \end{bmatrix} \begin{bmatrix} c^{n+1} \\ \mu^{n+1} \end{bmatrix} = \begin{bmatrix} \frac{c^n}{\Delta t} - u^{n+1} D_x c^n - v^{n+1} D_y c^n \\ (c^n)^3 \end{bmatrix} \tag{44}$$

Since the implicit approach is used in this study to solve the governing equations, the algorithm is unconditionally stable. The stability is unrestricted by the time step ($\Delta t$).

## 3. Results

### *3.1 Result on Mesh Independency Test*

The node independence test was conducted to ensure proper outcomes with independent value and stability based on time evolution and to get the optimum node quantity in this proposed numerical model. Independence test running under the $\Delta$t=0.0001, $\varepsilon$=0.1, $\sigma$=0.02 N/m, $\eta_1/\eta_2$= 0.5, $\rho_{oil}$=875 kg/m$^3$ and the $\rho_{water}$=1000 kg/m$^3$. Based on Figure 3, the numerical results remain constant when the number of nodes is increased. The x-axis and y-axis presented the node configuration and percent error of the collision times, respectively. The percent errors are obtained by comparing the collision times with the correlation obtained in Eq. (43). It is found that when using 151×151, 201×201, and 251×251 node configurations, the percent errors are almost the same. Accordingly, the 151×151 nodes are the optimum configuration used for the simulations. Furthermore, the shape parameter must be considered because each value produces different errors. Figure 4 represents the evaluation of various-shaped parameters to the produced error, in which the 0.1 in shape parameter has the lowest error with 1.03%. This produced errors for each shape parameter running under the optimum mesh configuration 151×151 that compares the gained collision time value with the earlier study [11]. The graph in this research has the same trendline as the available data in reference [26].

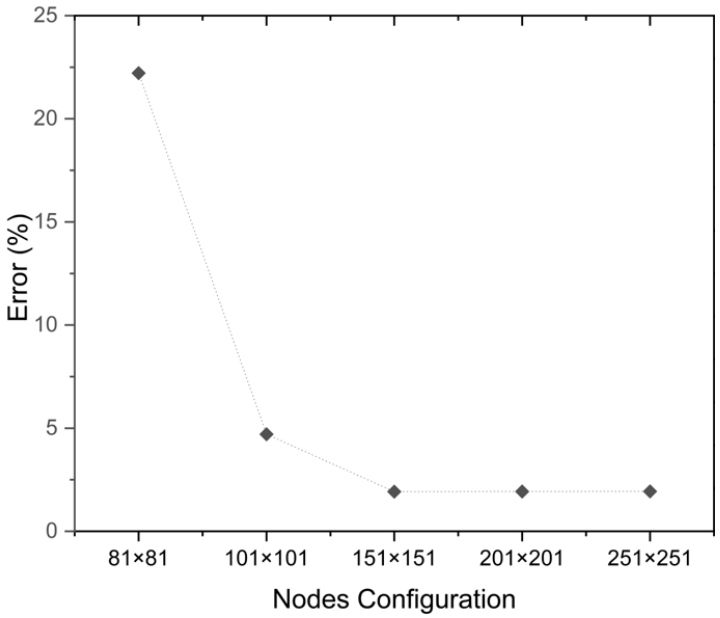


**Fig. 3.** Node independency test: obtain using five node configurations (81×81, 101×101, 151×151, 201×201, and 251×251)

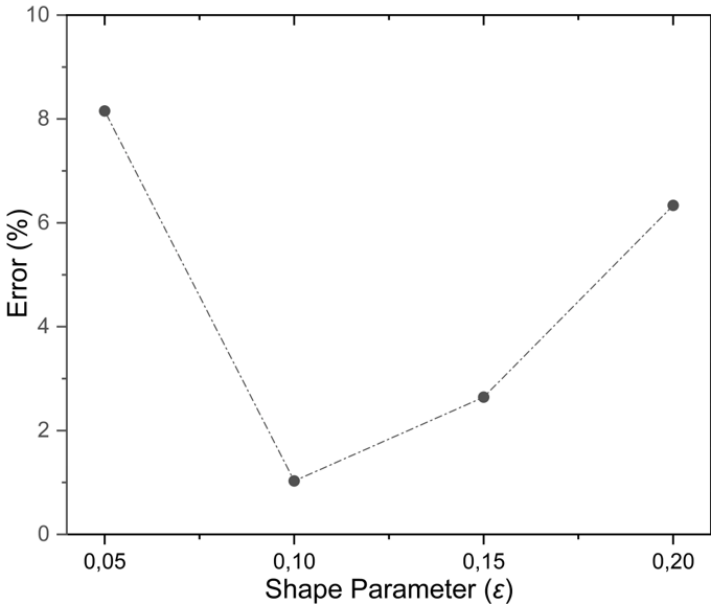


**Fig. 4.** The effect of shape parameter in resulting collision time error validated with the reference [11]

### *3.2 Numerical Validation*

In this study, the droplet coalescence was investigated numerically using the RBF method. The problem is governed by the Navier-Stokes and the Cahn-Hilliard equations for capturing the interface between two fluids. The pressure-velocity coupling in the momentum equations is solved using the fractional step method.

In order to validate the present numerical method, five simulations were done using five different surface tension ($\sigma$) values of 0.01, 0.02, 0.03, 0.04, and 0.05 N/m. In this case, the droplet on the right side is stagnant and the other droplet is moving toward with the velocity of 1 m/s. The other numerical parameters were considered as provided in Table 2. The obtained collision times were compared with the correlation proposed by Mohammadi *et al.,* [11]. The correlation to calculate the collision time is given as Eq. (45). where $Re = \rho_o VoDo/\eta_o$, $We = \rho_w Vo^2 Do/\sigma$, $\tau = tVo/Do$, and the constants are identified with $C_1 = 7.935E + 7$, $C_2 = -3.354$, $C_3 = 1.697E + 3$, and $C_4 = 0.2052$.

$$\tau = C_1 Re^{C_2} + C_3 We^{C_4} \tag{45}$$

**Table 2**
Numerical simulation parameters

| Parameter | Value |
|---|---|
| $D_o$ (µm) | 200 |
| $V_o$ (m/s) | 1.5 |
| $\sigma$ (N/m) | 0.028 |
| $\rho_w$ (kg/m$^3$) | 1000 |
| $\rho_o$ (kg/m$^3$) | 875 |
| $\eta_w$ (cP) | 1 |
| $\eta_o$ (cP) | 2 |

The comparisons of the collision time are shown in Figure 5. The maximum error is 3.59 % for a surface tension of 0.05 N/m. Based on that image, it is possible to conclude that the proposed model is well-suited to modelling droplet coalescence with reference data. Furthermore, the proposed numerical model was also validated with the outcomes proposed model authored by Mansouri *et al.,* In their simulation, two droplets are moving towards each other with the velocity of Vo (Figure 1), and hence Vo = 2Vo. Figure 6 reveals the deformation of the two colliding droplets at the specified time, and it is in good agreement with previous results in reference [12]. The simulation parameters are presented in Table 2.

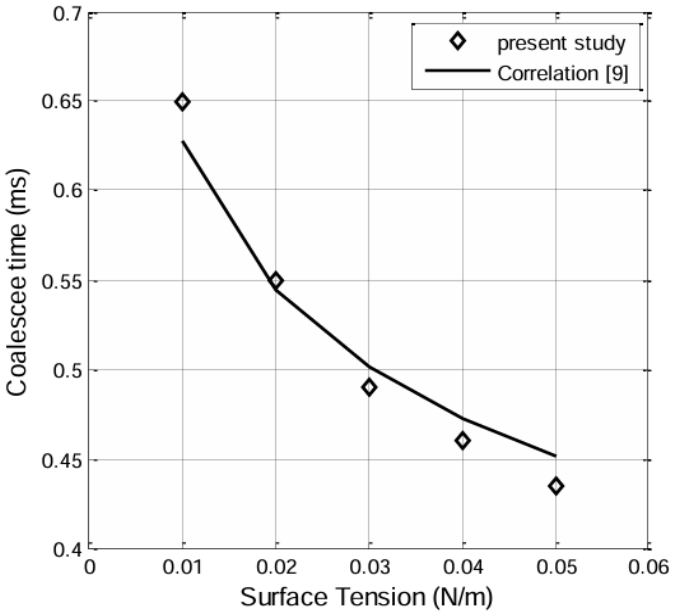


**Fig. 5.** Comparison of the collision time obtained in the present study and reference [11]

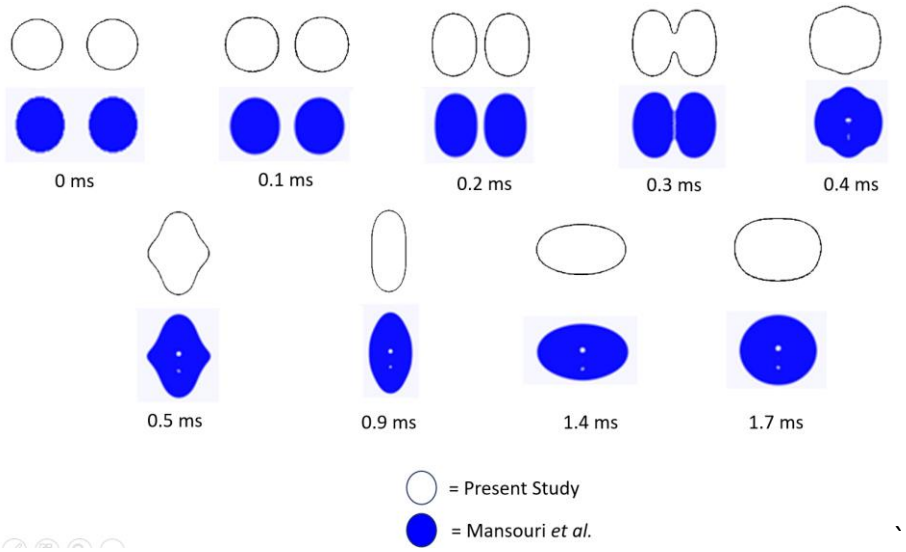


**Fig. 6.** Comparison of the collision sequence obtained in the present study and reference [12]

### *3.3 The Effects of Viscosity, Collision Velocity, and Surface Tension on the Coalescence Droplet*

The viscosity effects of the continuous phase (ηo) were investigated in the simulation under different values of 2, 4, and 8 cP. Figure 7 shows the deformation of the colliding droplet as the viscosity effect at the different collision times. The figure illustrates that increasing the viscosity delays the contact of two droplets and increases the collision time. There are merges after 4 ms for the 2 and 4 cP viscosities; on the other hand, 8 CP remains at 5 ms. The increase in viscosity values linearly increases the film thinning force which defines a resistant force against the approaching droplet movements. Therefore, the large value in viscosity highly influenced the coalescence time. Theoretically, the general high viscosity indicates the dense structure in the fluid molecular. When two droplets collide with the same initiation speed and viscosity but instead have a high density, the equilibrium mixing of molecules will take longer. This was noticeable at 8 cP when the fluid molecular merging process proceeded slower than others, particularly in the t = 0.4–0.5 ms range, resulting in a thicker fluid merging film.

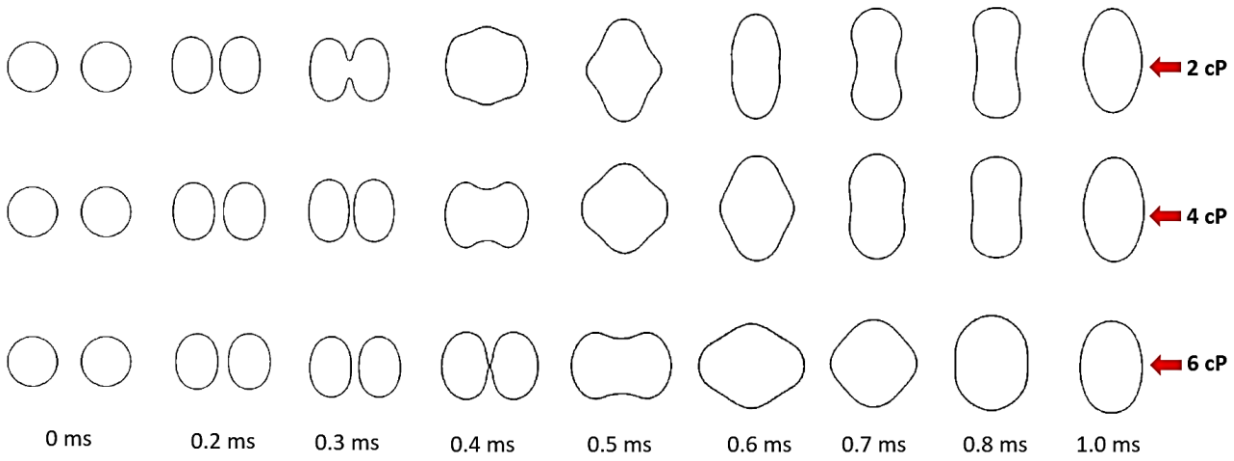


**Fig. 7.** The effect of viscosity on the coalescence of two droplets

The effect of collision velocity on the droplet coalescence is displayed in Figure 8. The simulation was performed for the collision velocities of Vo = 1.5 m/s and Vo = 3 m/s. In the droplet collision, kinetic energy is transformed into surface energy when two droplets merge and high pressure exists in both gaps. The flattened morphological interface occurred due to this condition. The two droplets contact each other at t = 0.177 ms for Vo = 3.0 m/s, and it takes place at t = 0.283 ms for Vo = 1.5 m/s. Based on the result, it was found that droplet collision time shorted when its velocity increased. Theoretically, when the droplets move slower, the pressure region between them is higher than when the droplets move faster. As a result, the coalescence process takes a longer time.

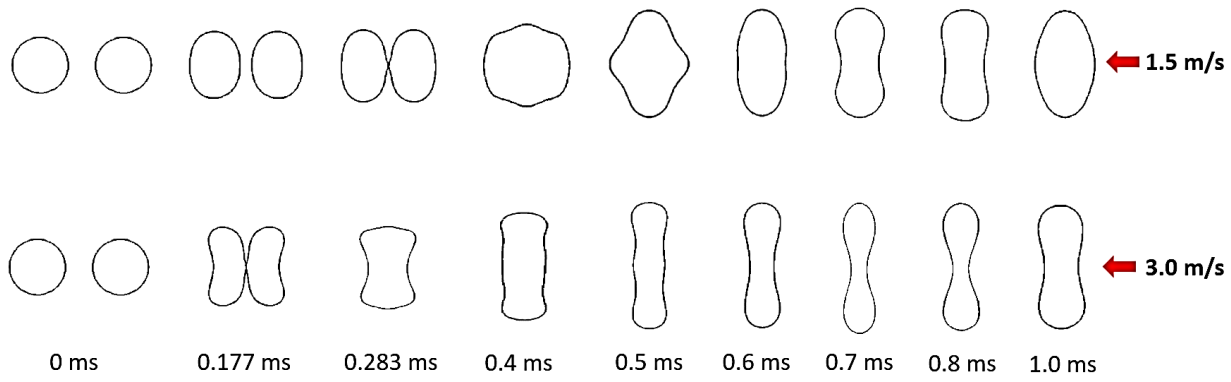


**Fig. 8.** The effect of velocity on the coalescence of two droplets

Surface tension is an essential parameter that must be considered in the droplet coalescence process. This parameter affects the equilibrium droplet shape and the interface molecular attraction force. Figure 9 illustrates the effect of surface tension on the collision time using different surface tension values of 0.014, 0.028, and 0.056 N/m. Based on the result, the fast collision time was linearly proportional to the increase in surface tension. The volumetric surface energy of the coalescence is established by the change in kinetic energy instantly before droplets merge. During the coalescence process, the changing pressure in both droplet regions is directly influenced by surface tension. Molecular attraction occurs when both droplets interface in a close position. As a result, the high molecular attraction occurs at a high surface tension value so the coalescence process was faster than the lower surface tension.

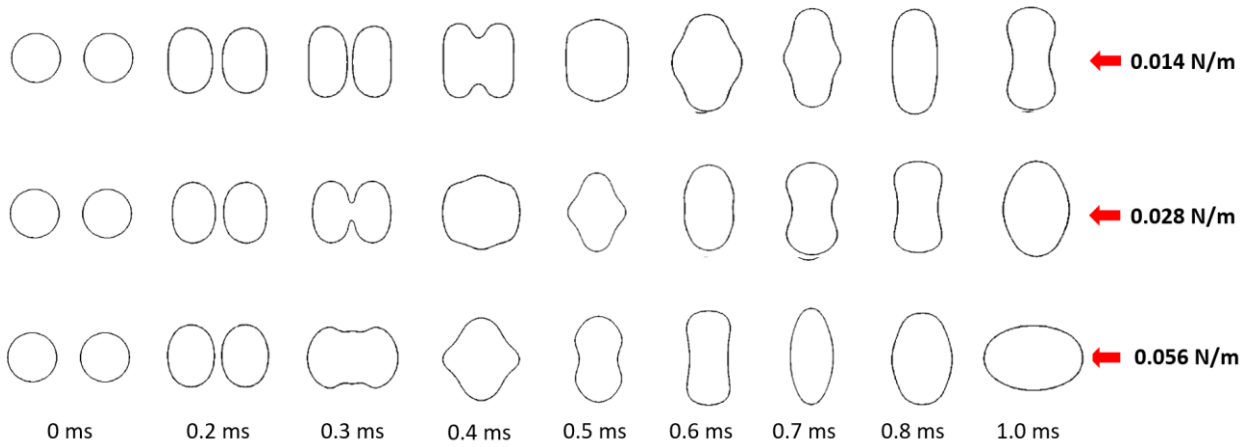


**Fig. 9.** The effect of surface tension on the coalescence of two droplets

### *3.4 Convergence Analysis and Analytical Solution*

The proposed radial basis function and combined domain decomposition method produce acceptable numerical results. The validity of its justification was strengthened by the calculated outcome of the root mean square of divergence. The equation for calculating the root mean square of divergence is provided by Eq. (46). Based on Figure 10, the graph illustrates the logarithm (base 10) of the root-mean-square of the divergence (LOGRMSDIV) as a function of time. The current numerical model has exceptional convergence, as indicated by the value of LOGRMSDIV being less than -4. This convergence analysis considered the RMSDIV also proposed in the earlier study

conducted by Rogers *et al.,* related to the study of the numerical simulation Navier-Stokes in 3D Curvilinear Coordinates [37].

$$RMSDIV = \sqrt{\frac{1}{N}\sum_{i=1}^{N}\left(\frac{\partial u_i}{\partial x}+\frac{\partial v_i}{\partial y}\right)^2} \tag{46}$$

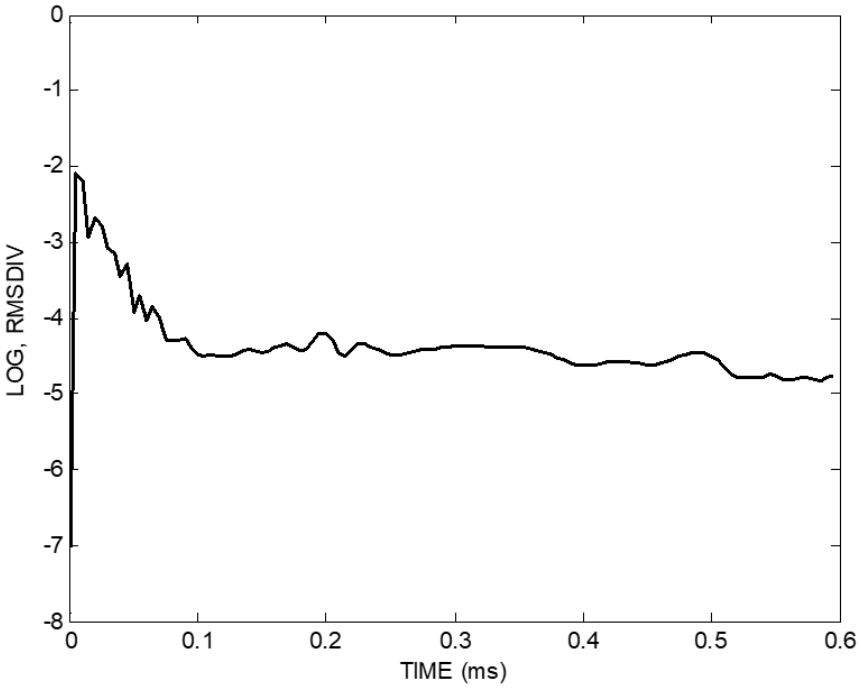


**Fig. 10.** The convergence history the model

To measure the error in the RBF-DDM approach, a test example of incompressible Navier-Stokes equations with a known analytical solution is examined. The governing equations of the test problem given by

$$\frac{\partial \mathbf{u}}{\partial t}+\mathbf{u}.\nabla\mathbf{u}-\frac{1}{Re}\nabla^2\mathbf{u}+\nabla p=\mathbf{0} \tag{47}$$

$$\nabla.\mathbf{u}=0 \tag{48}$$

Where *Re* is the Reynolds number. The analytical solutions of the test problem are given by

$$u(x,y,t)=-(\cos x\sin y)e^{-2t} \tag{49}$$

$$v(x,y,t)=(\sin x\cos y)e^{-2t} \tag{50}$$

$$p(x,y,t)=-\frac{Re}{4}(\cos 2x+\cos 2y)e^{-2t} \tag{51}$$

The test problem uses the square computational domain of $[0,\pi]\times[0,\pi]$ and *Re* = 1. Table 3 shows the errors obtained at times t = 0.5 and t = 1 using a node distribution of 41×41. RBF-DDM used the same quantity domain, but it was divided to become a 4×4 subdomain. To compare both methods, Eq. (52) calculates the root-mean-square of velocity (RMSU) for both RBF and RBF-DDM.

$$RMSU = \sqrt{\frac{1}{N}(u_i - ua_i)^2} \quad (52)$$

Where *N*, *u*, and *ua* are the number of nodes, approximate solution, and analytical solution, respectively. In terms of RMSU in the test problem, the RBF-DDM and global RBF have almost the same level of accuracy.

**Table 3**
The RMSU obtained using global RBF and RBF-DDM

| *t* | RMSU (RBF-DDM) | RMSU (RBF) |
|---|---|---|
| 0.5 | 8.1e-5 | 7.03e-5 |
| 1 | 3.0e-5 | 2.59e-5 |

## 4. Conclusions

A numerical study on the basis of the radial basis function method has been conducted to simulate the coalescence of water droplets in the oil. The Cahn-Hilliard equations were utilized to capture the interface between two fluids. The proposed numerical model was validated with the data available in the literature. The results obtained from the present study are in good agreement with the data available in the literature.

In the study, the effects of the viscosity of the continuous phase, surface tension, and collision velocity on the droplet coalescence were investigated numerically. The increase in viscosity increases the collision time, therefore postponing the contact between two droplets. It is also shown that an increase in surface tension and collision velocity produces shorter collision times. The present numerical model demonstrates the capability of the RBF method to solve droplet coalescence, and it can be extended to model coalescence processes in industrial contexts. In the next study, the present numerical method can be developed to solve many problems related to multiphase flow, such as rising bubbles, droplet evaporation, and liquid droplets impinging onto a hot surface. To ease the understanding of the RBF-DDM implemented method, the pseudocode for implementing the combination of RBF and domain decomposition method is available in our published article, which is related to using both methods in solving the KHI wave growth in slug flow [38].

## Acknowledgement
This research is supported by the Universitas Sebelas Maret (Grant: 254/UN27.22/HK.01.03/2022).

## References
[1] Jia, Wangcun, and H-H. Qiu. "Experimental investigation of droplet dynamics and heat transfer in spray cooling." *Experimental Thermal and Fluid Science* 27, no. 7 (2003): 829-838. https://doi.org/10.1016/S0894-1777(03)00015-3
[2] Dumka, Pankaj, and Dhananjay R. Mishra. "Performance evaluation of single slope solar still augmented with the ultrasonic fogger." *Energy* 190 (2020): 116398. https://doi.org/10.1016/j.energy.2019.116398
[3] Ashgriz, N., and P. Givi. "Coalescence efficiencies of fuel droplets in binary collisions." *International Communications in Heat and Mass Transfer* 16, no. 1 (1989): 11-20. https://doi.org/10.1016/0735-1933(89)90037-7
[4] Ashham, M., Ahmed Mohmad Aliywy, S. H. Raheemah, K. Salman, and M. Abbas. "Computational Fluid Dynamic Study on Oil-Water Two Phase Flow in A Vertical Pipe for Australian Crude Oil." *Journal of Advanced Research in Fluid Mechanics and Thermal Sciences* 71, no. 2 (2020): 134-142. https://doi.org/10.37934/arfmts.71.2.134142
[5] Mostaghimi, Javad, Sanjeev Chandra, Reza Ghafouri-Azar, and Ali Dolatabadi. "Modeling thermal spray coating processes: a powerful tool in design and optimization." *Surface and Coatings Technology* 163 (2003): 1-11. https://doi.org/10.1016/S0257-8972(02)00686-22

[6] Atten, Pierre, and Frédéric Aitken. "Electrocoalescence criterion for two close water drops." In *2007 IEEE Industry Applications Annual Meeting*, pp. 452-456. IEEE, 2007. https://doi.org/10.1109/07IAS.2007.7
[7] Nikolopoulos, N., A. Theodorakakos, and G. Bergeles. "Off-centre binary collision of droplets: A numerical investigation." *International Journal of Heat and Mass Transfer* 52, no. 19-20 (2009): 4160-4174. https://doi.org/10.1016/j.ijheatmasstransfer.2009.04.011
[8] Das Neves Gomes, Mateus, Elizaldo Domingues dos Santos, Liércio André Isoldi, and Luiz Alberto Oliveira Rocha. "Numerical analysis including pressure drop in oscillating water column device." *Open Engineering* 5, no. 1 (2015) : 229-237. https://doi.org/10.1515/eng-2015-0019
[9] Mason, Lachlan R., Geoffrey W. Stevens, and Dalton JE Harvie. "Multi-scale volume of fluid modelling of droplet coalescence." In *Ninth International Conference on CFD in the Minerals and Process Industries*. 2012.
[10] Pan, Kuo-Long, Chung K. Law, and Biao Zhou. "Experimental and mechanistic description of merging and bouncing in head-on binary droplet collision." *Journal of Applied Physics* 103, no. 6 (2008). https://doi.org/10.1063/1.2841055
[11] Mohammadi, Mehdi, Shahrokh Shahhosseini, and Mahmoud Bayat. "Direct numerical simulation of water droplet coalescence in the oil." *International Journal of Heat and Fluid Flow* 36 (2012): 58-71. https://doi.org/10.1016/j.ijheatfluidflow.2012.04.001
[12] Mansouri, A., H. Arabnejad, and R. S. Mohan. "Numerical investigation of droplet-droplet coalescence and droplet-interface coalescence." In *Fluids Engineering Division Summer Meeting*, vol. 46216, p. V01AT05A006. American Society of Mechanical Engineers, 2014. https://doi.org/10.1115/FEDSM2014-21642
[13] Hoffmann, Klaus A., and Steve T. Chiang. "Computational fluid dynamics volume I." *Engineering education system* (2000).
[14] Moukalled, Fadl, Luca Mangani, Marwan Darwish, F. Moukalled, L. Mangani, and M. Darwish. *The finite volume method*. Springer International Publishing, 2016. https://doi.org/10.1007/978-3-319-16874-6
[15] Kwon, Young W., and Hyochoong Bang. *The finite element method using MATLAB*. CRC press (2018). https://doi.org/10.1201/9781315275949
[16] Perepechko, Yury, Konstantin Sorokin, and Kholmatzhon Imomnazarov. "Numerical simulation of the free convection in a viscous compressible fluid." *Open Engineering* 6, no. 1 (2016). https://doi.org/10.1515/eng-2016-0084
[17] Atluri, Satya N., and Tulong Zhu. "A new meshless local Petrov-Galerkin (MLPG) approach in computational mechanics." *Computational mechanics* 22, no. 2 (1998): 117-127. https://doi.org/10.1007/s004660050346
[18] Buhmann, Martin Dietrich. "Radial basis functions." *Acta numerica* 9 (2000): 1-38. https://doi.org/10.1017/CBO9780511543241
[19] Najafi, Mohammad, and Vali Enjilela. "Natural convection heat transfer at high Rayleigh numbers–Extended meshless local Petrov–Galerkin (MLPG) primitive variable method." *Engineering Analysis with Boundary Elements* 44 (2014): 170-184. https://doi.org/10.1016/j.enganabound.2014.01.022
[20] Mai-Duy, Nam, and Thanh Tran-Cong. "An efficient indirect RBFN-based method for numerical solution of PDEs." *Numerical Methods for Partial Differential Equations: An International Journal* 21, no. 4 (2005): 770-790. https://doi.org/10.1002/num.20062
[21] Yun-Xin, Zhang, and Tan Yong-Ji. "Meshless schemes for unsteady Navier–Stokes equations in vorticity formulation using radial basis functions." *Journal of computational and applied mathematics* 192, no. 2 (2006): 328-338. https://doi.org/10.1016/j.cam.2005.05.011
[22] Ma, Menglong, Jun Xu, Jun Lu, and Ji Lin. "The novel backward substitution method for the simulation of three-dimensional time-harmonic elastic wave problems." Applied Mathematics Letters 150 (2024): 108963. https://doi.org/10.1016/j.aml.2023.108963
[23] Zhang, Yuhui, Timon Rabczuk, Ji Lin, Jun Lu, and C. S. Chen. "Numerical simulations of two-dimensional incompressible Navier-Stokes equations by the backward substitution projection method." *Applied Mathematics and Computation* 466 (2024): 128472. https://doi.org/10.1016/j.amc.2023.128472
[24] Zheng, Jing, Shengfeng Zhu, and Fazlollah Soleymani. "A new efficient parametric level set method based on radial basis function-finite difference for structural topology optimization." Computers & Structures 297 (2024): 107364. https://doi.org/10.1016/j.compstruc.2024.107364
[25] Soleymani, Fazlollah, and Shengfeng Zhu. "RBF-FD solution for a financial partial-integro differential equation utilizing the generalized multiquadric function." *Computers & Mathematics with Applications* 82 (2021): 161-178. https://doi.org/10.1016/j.camwa.2020.11.010
[26] Soleymani, Fazlollah, and Shengfeng Zhu. "Error and stability estimates of a time-fractional option pricing model under fully spatial–temporal graded meshes." *Journal of Computational and Applied Mathematics* 425 (2023): 115075. https://doi.org/10.1016/j.cam.2023.115075
[27] Pepper, Darrell W., Xiuling Wang, and David B. Carrington. "A meshless method for modeling convective heat transfer." *Journal of heat transfer* 135, no. 1 (2013): 011003. https://doi.org/10.1115/1.4007650

[28] Barosan, I., P. D. Anderson, and H. E. H. Meijer. "Application of mortar elements to diffuse-interface methods." *Computers & fluids* 35, no. 10 (2006): 1384-1399. https://doi.org/10.1016/j.compfluid.2005.06.005
[29] Lee, Hyun Geun, and Junseok Kim. "Two-dimensional Kelvin–Helmholtz instabilities of multi-component fluids." *European Journal of Mechanics-B/Fluids* 49 (2015): 77-88. https://doi.org/10.1016/j.euromechflu.2014.08.001
[30] Bates, Peter W., and Paul C. Fife. "The dynamics of nucleation for the Cahn–Hilliard equation." *SIAM Journal on Applied Mathematics* 53, no. 4 (1993): 990-1008. https://doi.org/10.1137/0153049
[31] Anderson, Daniel M., Geoffrey B. McFadden, and Adam A. Wheeler. "Diffuse-interface methods in fluid mechanics." *Annual review of fluid mechanics* 30, no. 1 (1998): 139-165. https://doi.org/10.1146/annurev.fluid.30.1.139
[32] Kansa, Edward J. "Multiquadrics—A scattered data approximation scheme with applications to computational fluid-dynamics—I surface approximations and partial derivative estimates." *Computers & Mathematics with applications* 19, no. 8-9 (1990): 127-145. https://doi.org/10.1016/0898-1221(90)90270-T
[33] Santosa, Irfan, Eko Prasetya Budiana, Syamsul Hadi, and Agung Tri Wijayanta. "Laminar Rayleigh–Benard convection in a closed square field with meshless radial basis function method." *Curved and Layered Structures* 10, no. 1 (2023): 20220204. https://doi.org/10.1515/cls-2022-0204
[34] Ouertatani, Nasreddine, Nader Ben Cheikh, Brahim Ben Beya, and Taieb Lili. "Numerical simulation of two-dimensional Rayleigh–Bénard convection in an enclosure." *Comptes Rendus Mécanique* 336, no. 5 (2008): 464-470. https://doi.org/10.1016/j.crme.2008.02.004
[35] Ling, Leevan, and Edward J. Kansa. "Preconditioning for radial basis functions with domain decomposition methods." *Mathematical and Computer modelling* 40, no. 13 (2004): 1413-1427. https://doi.org/10.1016/j.mcm.2005.01.002
[36] Budiana, Eko Prasetya. "Meshless numerical model based on radial basis function (RBF) method to simulate the Rayleigh–Taylor instability (RTI)." *Computers & Fluids* 201 (2020): 104472. https://doi.org/10.1016/j.compfluid.2020.104472
[37] Rogers, Stuart E., Dochan Kwak, and James LC Chang. *Numerical solution of the incompressible Navier-Stokes equations in three-dimensional generalized curvilinear coordinates*. No. NAS 1.15: 86840. 1986.
[38] Budiana, Eko Prasetya. "The meshless numerical simulation of Kelvin–Helmholtz instability during the wave growth of liquid–liquid slug flow." *Computers & Mathematics with Applications* 80, no. 7 (2020): 1810-1838. https://doi.org/10.1016/j.camwa.2020.08.006